Available online at www.sciencedirect.com
ScienceDirect
International Journal of Solids and Structures 44 (2007) 4784–4794
INTERNATIONAL JOURNAL OF SOLIDS and STRUCTURES
www.elsevier.com/locate/ijsolstr

Wave propagation and the frequency domain Green's functions in viscoelastic Biot/squirt (BISQ) media

Dinghui Yang [a], Yiqing Shen [b], Enru Liu [c,d,*]

[a] Department of Mathematical Sciences, Tsinghua University, Beijing 100084, China
[b] LHD, Institute of Mechanics, Chinese Academy of Sciences, Beijing 100080, China
[c] British Geological Survey, Murchison House, West Mains Road, Edinburgh EH9 3LA, Scotland, UK
[d] Department of Geophysics, China University of Mining and Technology, Xuzhou, China

Received 18 November 2005; received in revised form 11 October 2006
Available online 8 December 2006

Abstract

In this paper, we examine the characteristics of elastic wave propagation in viscoelastic porous media, which contain simultaneously both the Biot-flow and the squirt-flow mechanisms (BISQ). The frequency-domain Green's functions for viscoelastic BISQ media are then derived based on the classic potential function methods. Our numerical results show that S-waves are only affected by viscoelasticity, but not by squirt-flows. However, the phase velocity and attenuation of fast P-waves are seriously influenced by both viscoelasticity and squirt-flows; and there exist two peaks in the attenuation-frequency variations of fast P-waves. In the low-frequency range, the squirt-flow characteristic length, not viscoelasticity, affects the phase velocity of slow P-waves, whereas it is opposite in the high-frequency range. As to the contribution of potential functions of two types of compressional waves to the Green's function, the squirt-flow length has a small effect, and the effects of viscoelastic parameter are mainly in the higher frequency range.

Keywords: Biot/squirt (BISQ) model; Poroelasticity; Viscoelastic media; Wave propagation; Green's function

1. Introduction

The Green's function is very useful and important in seismology, earthquake engineering, soil mechanics, geophysics, dynamic foundation theory, and other subjects. The Green's function can be used to derive representation integrals for the radiation from an arbitrary distribution of body forces and surface tractions, and can be applied to acoustic theory and numerical computations of many fields (Tewary, 1998; Spies, 1997; Liu et al., 2002; Liu and Zhang, 2001; Dravinski and Zheng, 2000). Green's functions have been derived for two-phase porous media. Norris (1985) found the formal solution of fast and slow dilation spectrum and distortion spectrum of the Green's function in two-phase saturated media. Kazi-Aoual et al. (1988) derived the Green's

* Corresponding author. Tel.: +44 131 650 0362; fax: +44 131 667 1877.
E-mail addresses: dhyang@math.tsinghua.edu.cn (D. Yang), yqshen@imech.ac.cn (Y. Shen), E.Liu@bgs.ac.uk, eliu0103@hotmail.com (E. Liu).

0020-7683/$ - see front matter
doi:10.1016/j.ijsolstr.2006.12.001

functions of infinite transversely isotropic saturated poroelastic media. Ding et al. (2001) obtained the Green's function for the two-phase saturated media for a concentrated force through dividing the force potential field and using the properties of the Dirac function.

In 1993, Dvorkin and Nur (1993) proposed a consistent Biot/squirt (BISQ) model, which combines the original Biot two-phase model (Biot, 1956) and the squirt-flow model proposed by Mavko and Nur (1975). In other words, the BISQ theory contains both the Biot (global)-flow and squirt (local)-flow mechanisms. Recently, Yang and Zhang (2000, 2002) extended the BISQ model to general anisotropic media. More recently, Cheng et al. (2002) presented a viscoelastic Biot/squirt model by introducing a viscoelastic stress strain constitutive relationship of solid phases, and found that the viscoelastic property of rocks, not the squirt-flow, causes the dispersion and attenuation in the low-frequency range.

In this paper, we derive the equations of phase velocities and attenuations of two compressional waves (fast P- and slow P-waves) and one rotational wave in terms of the decomposition of wave-fields of viscoelastic porous media. We further investigate the effects of squirt-flow characteristic parameters and viscoelasticity of solid phase on the phase velocity and attenuation of three body waves. Finally, we derive the Green's functions of the viscoelastic BISQ media using the classic potential function methods.

2. Wave propagation in viscoelastic BISQ media

Following Cheng et al. (2002), the wave equations in two-phase isotropic viscoelastic media can be written as

$$\begin{cases} \mu^*\nabla^2 u + \left(\lambda^* + \mu^* + \frac{a_{11}-\phi}{\phi} a_{11}F_1S_1\right)\nabla\nabla\cdot u + a_{11}F_1S_1\nabla\nabla\cdot U = \frac{\partial^2}{\partial t^2}(\rho_1 u + \rho_2 U) \\ \nabla[F_1S_1(a_{11}-\phi)\nabla\cdot u + \phi F_1S_1\nabla\cdot U] = \frac{\partial^2}{\partial t^2}(\rho_{12}u + \rho_{22}U) + \frac{\eta\phi^2}{k_{11}}\frac{\partial}{\partial t}(U-u), \end{cases} \tag{1}$$

where $\rho_{12} = -\rho_a$, $\rho_{22} = \phi\rho_f + \rho_a$, $\rho_1 = (1-\phi)\rho_s$, $\rho_2 = \phi\rho_f$. ρ_s is the density of the solid, ρ_f the density of the fluid, ϕ the porosity of the rock; η is the viscosity of the fluid, ρ_a is the additional coupling density, and k_{11} is the permeability. α_{11} is the viscoelastic coefficient of the effective stress. ∇ is the Hamilton operator, $u = (u_x, u_y, u_z)^T$ and $U = (U_x, U_y, U_z)^T$ in which u_i and U_i $(i = 1, 2, 3)$ denote, respectively, displacement components of the solid and the fluid in the i-direction. λ^* and μ^* are the viscoelastic coefficients. F_1 is the Biot-flow coefficient and S_1 is the squirt-flow coefficient (Dvorkin and Nur, 1993)

$$S_1 = 1 - \frac{2J_1(\lambda_1 R)}{\lambda_1 R J_0(\lambda_1 R)}, \quad \text{and} \quad \lambda_1^2 = \frac{\rho_f\omega^2}{F_1}\left(\frac{\phi + \rho_a/\rho_f}{\phi} + i\frac{\eta\phi}{\rho_f\omega k_{11}}\right).$$

where J_0 and J_1 are the Bessel functions of the zeroth-order and first-order, respectively; the parameter R represents the average characteristic squirt-flow length.

The Fourier transformed stress–strain constitutive relationship of steady states is

$$\sigma(t) = G^*(\omega)\cdot\varepsilon_0 e^{i\omega t},$$

where ε_0 is a constant strain tensor, G^* denotes the complex modulus (in isotropic media, $G^* = (\mu^*, \lambda^*)^T$). The moduli are determined as follows

$$\tan\delta = G''/G',$$
$$G'(\omega) = G_0'\left[1 + \frac{\tan\delta}{\pi}\ln\left(\frac{\omega}{\omega_0}\right)\right],$$
$$G^*(\omega) = G'(\omega) + iG''(\omega),$$

where ω_0 is the reference frequency and G_0' is the elastic modulus.

We define the following notations:

$$e = \nabla\cdot u, \quad \varepsilon = \nabla\cdot U,$$
$$\varpi = \nabla\times u, \quad \Omega = \nabla\times U.$$

Applying the curl operator to Eq. (1), we have

$$\begin{cases} \mu\nabla^2\varpi = \frac{\partial^2}{\partial t^2}(\rho_1\varpi + \rho_2\Omega) \\ 0 = \frac{\partial^2}{\partial t^2}(\rho_{12}\varpi + \rho_{22}\Omega) + \frac{\eta\phi^2}{k_{11}}\frac{\partial}{\partial t}(\Omega - \varpi). \end{cases} \tag{2}$$

Without the loss of generality, for a plane wave, the magnitude of rotations of solid and fluid in the z-direction may be written as

$$\begin{cases} \varpi = C_1 e^{i(kx-\omega t)} \\ \Omega = C_2 e^{i(kx-\omega t).} \end{cases} \tag{3}$$

Substituting Eq. (3) into Eq. (2) and eliminating C_1 and C_2, we obtain

$$k^2\tilde{\rho}_{22}\mu^* = \omega^2(\rho_1\tilde{\rho}_{22} - \rho_2\tilde{\rho}_{12}), \tag{4}$$

where $\tilde{\rho}_{12}$, $\tilde{\rho}_{22}$, and μ^* are complex quantities, and

$$\tilde{\rho}_{12} = \rho_{12} - i\frac{\eta\phi^2}{k_{11}\omega}, \quad \tilde{\rho}_{22} = \rho_{22} + i\frac{\eta\phi^2}{k_{11}\omega}.$$

Substituting $k = k_r + ik_i$, phase velocity v_s and attenuation are given by

$$v_s = \omega/k_r, \quad \text{and} \quad Q_s^{-1} = 2k_i/k_r, \tag{5}$$

where k_r and k_i can be obtained from Eq. (4). There is only one rotational wave. We can find the relationship between the rotation ϖ of solids and the rotation Ω of fluids:

$$\Omega = -\frac{\tilde{\rho}_{12}}{\tilde{\rho}_{22}}\varpi.$$

Let the fluid and solid displacements satisfy the relation $U = \xi u$, then for the shear waves, we have

$$\xi_S = -\tilde{\rho}_{12}/\tilde{\rho}_{22}. \tag{6}$$

From Eqs. (4) and (5), we find that the variables v_s, Q_s^{-1}, and ξ_s are not related to the squirt-flow coefficient S_1, and that the shear waves are not affected by the squirt-flow in porous isotropic viscoelastic media. The expressions for $\tilde{\rho}_{12}$ and $\tilde{\rho}_{22}$ indicate that the ratio ξ_s is independent of viscoelasticity of solid phases.

In all numerical examples presented in this paper except where stated otherwise, the following input parameters are used: $\rho_s = 2650$ kg/m^3, $\rho_f = 1000$ kg/m^3, $\rho_a = 420$ kg/m^3, $K_S = 38$ GPa, $V_f = 1500$ m/s, $\tilde{V}_P = 3969$ m/s, $\tilde{V}_S = 2547$ m/s, $\phi = 0.15$, $k_{11} = 1.25$ mD, $\eta = 0.01$ ps, $\omega_0 = 1000$ Hz, $R = 0.5$ mm, 1 mm, 5 mm and $\tan\delta = 0.001$, 0.035, 0.05.

In all figures in this paper, different solid lines correspond to different values of R with $\tan\delta = 0.035$; different dashed lines correspond to different values of $\tan\delta$ with $R = 5$ mm. If R is not given in a figure, it means that the curves for the value of R and the curve with $\tan\delta = 0.035$ overlap. If $\tan\delta$ is not given in a figure, it means that the curves for different values of $\tan\delta$ and the curve with $R = 5$ mm overlap.

Figs. 1 and 2 show the variations of v_s and Q_s^{-1} with different parameters. From Fig. 1 we can see that for $\omega < \omega_0$ (ω_0 is the reference frequency) the phase velocity of S-waves decreases with increasing $\tan\delta$, but it decreases when $\omega > \omega_0$. In the low-frequency range, the inverse of quality factor Q_s^{-1} is not sensitive to frequency. However, in the high-frequency range, there exists a peak in Q_s^{-1}. When $\tan\delta$ is large, Q_s^{-1} is also large (Fig. 2). Figs. 1 and 2 show that the phase velocities and attenuations of S-waves are only affected by viscoelasticity.

Let

$$A_{11} = \lambda^* + 2\mu^* + \frac{a_{11} - \phi}{\phi}a_{11}F_1S_1, \quad A_{12} = a_{11}F_1S_1,$$
$$A_{21} = F_1S_1(a_{11} - \phi), \quad A_{22} = \phi F_1S_1.$$

Applying the divergence operator to Eq. (1), we obtain

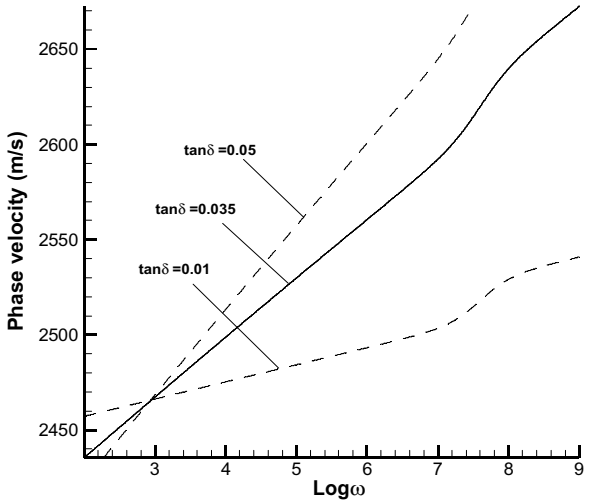

Fig. 1. Phase velocity of S-waves. Different solid lines correspond to different values of R with $\tan\delta = 0.035$; different dashed lines correspond to different values of $\tan\delta$ with $R = 5$ mm. If R is not given in a figure, it means that the curves for the value of R and the curve with $\tan\delta = 0.035$ overlap. If $\tan\delta$ is not given in a figure, it means that the curves for different values of $\tan\delta$ and the curve with $R = 5$ mm overlap.

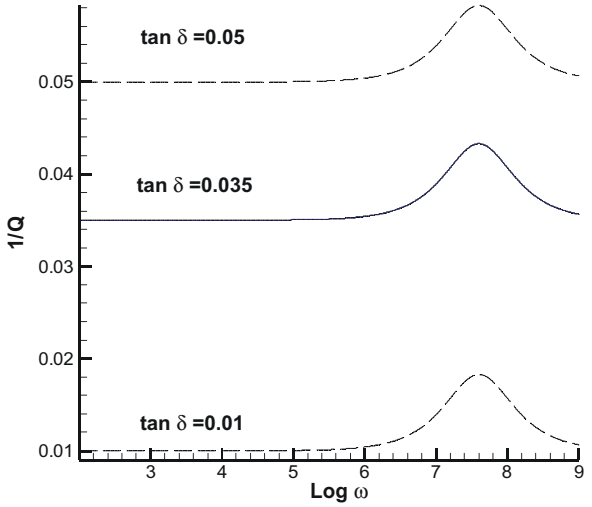

Fig. 2. The attenuation of S-waves. Different solid lines correspond to different values of R with $\tan\delta = 0.035$; different dashed lines correspond to different values of $\tan\delta$ with $R = 5$ mm. If R is not given in a figure, it means that the curves for the value of R and the curve with $\tan\delta = 0.035$ overlap. If $\tan\delta$ is not given in a figure, it means that the curves for different values of $\tan\delta$ and the curve with $R = 5$ mm overlap.

$$\begin{cases} A_{11}\nabla^2 e + A_{12}\nabla^2\varepsilon = \frac{\partial^2}{\partial t^2}(\rho_1 e + \rho_2\varepsilon) \\ A_{21}\nabla^2 e + A_{22}\nabla^2\varepsilon = \frac{\partial^2}{\partial t^2}(\rho_{12} e + \rho_{22}\varepsilon) + \frac{\eta\phi^2}{k_{11}}\frac{\partial}{\partial t}(\varepsilon - e). \end{cases} \tag{7}$$

Again we consider plane waves of the following form:

$$\begin{cases} e = C_1 \mathrm{e}^{\mathrm{i}(kx-\omega t)} \\ \varepsilon = C_2 \mathrm{e}^{\mathrm{i}(kx-\omega t)}. \end{cases} \tag{8}$$

Substituting Eq. (8) into Eq. (7), we obtain

$$\begin{cases} C_1A_{11}z + C_2A_{12}z = C_1\rho_1 + C_2\rho_2 \\ C_1A_{21}z + C_2A_{22}z = C_1\tilde{\rho}_{12} + C_2\tilde{\rho}_{22}. \end{cases} \tag{9}$$

where $z = k^2/\omega^2$. Eliminating C_1 and C_2, we have

$$(A_{11}A_{22} - A_{12}A_{21})z^2 - (\rho_1A_{22} + \tilde{\rho}_{22}A_{11} - \rho_2A_{21} - \tilde{\rho}_{12}A_{12})z + (\rho_1\tilde{\rho}_{22} - \rho_2\tilde{\rho}_{12}) = 0. \tag{10}$$

We can find two roots z_1 and z_2 from Eq. (10) and then obtain k_1 and k_2. The velocity v_i and the inverse quality factor Q_i^{-1} of these waves are given by

$$v_i = \omega/\mathrm{real}(k_i), \quad Q_i^{-1} = 2\,\mathrm{Imag}\,(k_i)/\mathrm{Real}(k_i) \quad (i = 1, 2), \tag{11}$$

where v_1 and v_2 are the velocities of the fast- and slow-dilatational waves (fast P- and slow P-waves), respectively. It is easy to see that the coefficients in Eq. (10) contain both the Biot-flow coefficient F_1 and the squirt-flow coefficient S_1, indicating that the velocities of fast and slow P-waves are affected not only by the Biot-flow, but also by the squirt-flow.

From Eqs. (8) and (9), we can obtain the following relationships of the fast P- and slow P-waves

$$\varepsilon_i = \xi_i e_i, \quad \xi_i = \frac{A_{11}z_i - \rho_1}{\rho_2 - A_{12}z_i} \quad \text{or} \quad \xi_i = \frac{A_{21}z_i - \tilde{\rho}_{12}}{\tilde{\rho}_{22} - A_{22}z_i} \quad (i = 1, 2). \tag{12}$$

Similarly, the fluid and solid displacements satisfy the relationship $U_i = \xi_i u_i$. Eq. (12) shows that, for a plane wave, the ratios of fluid to solid displacements ξ_i depend on the Biot-flow coefficient F_1 and the squirt-flow coefficient S_1, i.e., the ratios of fluid to solid displacements of the fast and slow P-waves are affected simultaneously by the Biot- and squirt-flow mechanisms. The ratios are also related to the viscoelasticity of the solid phase.

Figs. 3 and 4 show the effects of different parameters on phase velocity v_1 and attenuation Q_1^{-1} of fast P-wave. Fig. 3 shows that the phase velocity of fast P-waves increases with $\log\omega$, and when $\omega < \omega_0$ (ω_0 is the reference frequency), it decreases as $\tan\delta$ increases and it increases when $\omega > \omega_0$. From Fig. 3, we also can see that the zone of increas in the phase velocity of fast P-waves shifts towards low frequencies as R increases. In the high frequency range, those lines with different values of R overlap, indicating that the phase velocity of fast P-waves is mainly affected by the viscoelasticity of solid phases rather than the squirt-flow.

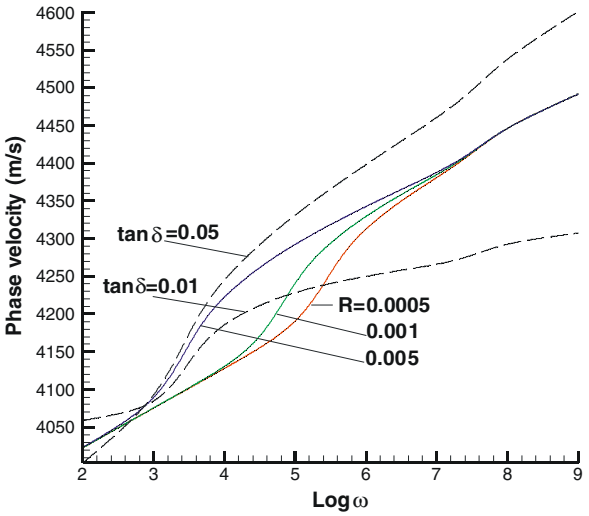

Fig. 3. Phase velocity of fast P-waves. Different solid lines correspond to different values of R with $\tan\delta = 0.035$; different dashed lines correspond to different values of $\tan\delta$ with $R = 5$ mm. If R is not given in a figure, it means that the curves for the value of R and the curve with $\tan\delta = 0.035$ overlap. If $\tan\delta$ is not given in a figure, it means that the curves for different values of $\tan\delta$ and the curve with $R = 5$ mm overlap.

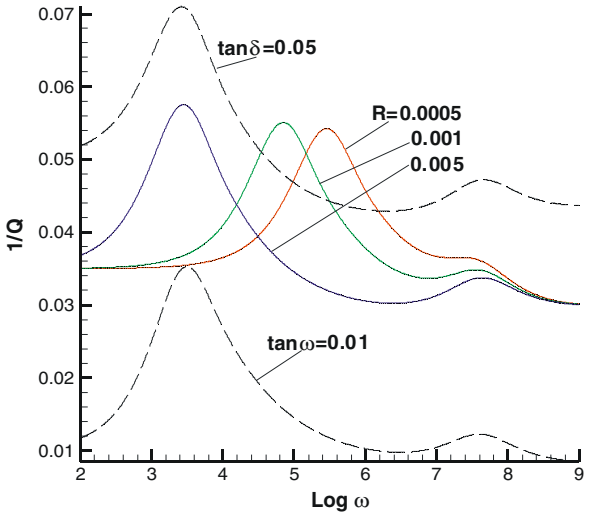

Fig. 4. The attenuation of the fast P-waves. Different solid lines correspond to different values of R with $\tan\delta = 0.035$; different dashed lines correspond to different values of $\tan\delta$ with $R = 5$ mm. If R is not given in a figure, it means that the curves for the value of R and the curve with $\tan\delta = 0.035$ overlap. If $\tan\delta$ is not given in a figure, it means that the curves for different values of $\tan\delta$ and the curve with $R = 5$ mm overlap.

The variations of attenuation Q_1^{-1} with frequency are given in Fig. 4. We can see there exist two attenuation peaks. For the lines with the same value of R and different values of $\tan\delta$ in Fig. 4, we find that the larger the value of $\tan\delta$, the larger the value of Q_1^{-1} is. Note that the two peaks are in the same frequency range. For the lines with the same value of $\tan\delta$ and different values of R, the first attenuation peak shifts towards low frequency as R increases, and passing the second attenuation peak, these attenuation lines are overlapped. Fig. 4 also shows the effects of viscoelasticity on the attenuation at all frequencies, and in contrast, the squirt-flow has a much less effect on the attenuation in the high frequency range.

Figs. 5 and 6 show that the effects of different parameters on the phase velocity v_2 and attenuation Q_2^{-1}. Fig. 5 shows that the velocity of slow P-waves varies from its low-frequency limit to the high-frequency limit as frequency increases. In the lower frequency range, the velocity v_2 is mainly affected by the parameter R rather than the parameter $\tan\delta$; while in the higher frequency range, the case is opposite. Fig. 6 shows that, in the low-frequency range, the attenuation of the slow P-wave (the value of Q_2^{-1}) is very large. The fact that those lines with different values of $\tan\delta$ overlap is an indication that Q_2^{-1} is mainly affected by R.

3. The Green's function

We now consider a time harmonic motion with a real frequency ω. Let

$$\begin{cases} u(x,y,z,t) = u(x,y,z)\mathrm{e}^{-\mathrm{i}\omega t} \\ U(x,y,z,t) = U(x,y,z)\mathrm{e}^{-\mathrm{i}\omega t}. \end{cases} \tag{13}$$

Let a point force with a unit amplitude, $F = \delta(x-\varsigma)K$ (δ is the Dirac function, K is the unit vector of the force), act at the ς position in the solid phase, then the equations of motion, after substituting Eq. (13) into Eq. (1), can be rewritten as

$$\begin{cases} \omega^2(\rho_1 u + \rho_2 U) + \mu^*\nabla^2 u + \left(\lambda^* + \mu^* + \frac{a_{11}^- \phi}{\phi} a_{11}F_1S_1\right)\nabla\nabla\cdot u + a_{11}F_1S_1\nabla\nabla\cdot U = -\delta(x-\varsigma)K \\ \omega^2(\tilde{\rho}_{12}u + \tilde{\rho}_{22}U) + \nabla(F_1S_1(a_{11}-\phi)\nabla\cdot u + \phi F_1S_1\nabla\cdot U) = 0. \end{cases} \tag{14}$$

Let $r = |x-\varsigma|$, the force F can be written as

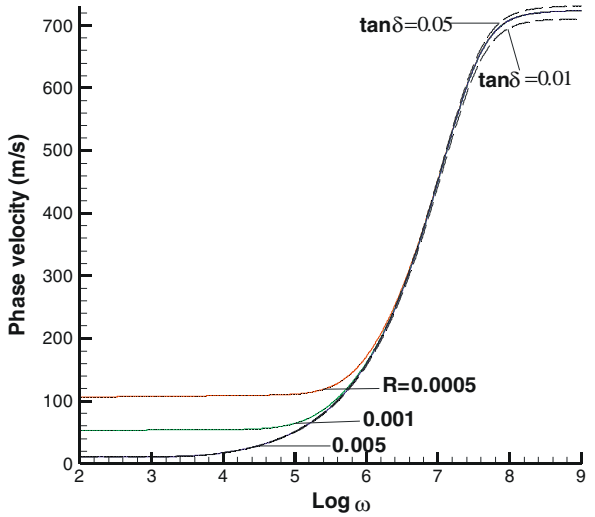

Fig. 5. Phase velocity of slow P-waves. Different solid lines correspond to different values of R with $\tan\delta = 0.035$; different dashed lines correspond to different values of $\tan\delta$ with $R = 5$ mm. If R is not given in a figure, it means that the curves for the value of R and the curve with $\tan\delta = 0.035$ overlap. If $\tan\delta$ is not given in a figure, it means that the curves for different values of $\tan\delta$ and the curve with $R = 5$ mm overlap.

$$K\delta(x-\varsigma) = -\frac{K}{4\pi}\nabla^2\left(\frac{1}{r}\right) = -\frac{1}{4\pi}\left[\nabla\nabla\cdot\left(\frac{K}{r}\right) - \nabla\times\nabla\times\left(\frac{K}{r}\right)\right]. \tag{15}$$

Applying the curl operator to Eq. (14), and then combining with Eq. (4), we can obtain

$$\nabla^2\nabla\times u + k_S^2\nabla\times u = \frac{-1}{4\pi V_S^2[(\rho_1\tilde{\rho}_{22} - \tilde{\rho}_{12}\rho_2)/\tilde{\rho}_{22}]}\nabla\times\nabla\times\nabla\times\left(\frac{K}{r}\right), \tag{16}$$

where $k_S = \omega/V_S$ is the shear wave number. If there is a potential function Ψ_s, satisfies

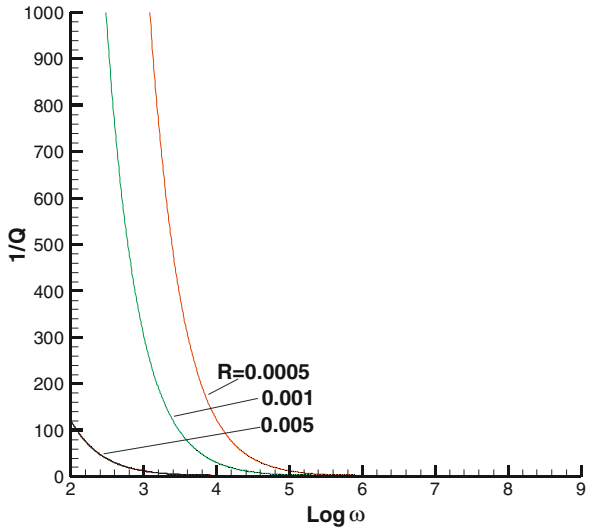

Fig. 6. The attenuation of the slow P-waves. Different solid lines correspond to different values of R with $\tan\delta = 0.035$; different dashed lines correspond to different values of $\tan\delta$ with $R = 5$ mm. If R is not given in a figure, it means that the curves for the value of R and the curve with $\tan\delta = 0.035$ overlap. If $\tan\delta$ is not given in a figure, it means that the curves for different values of $\tan\delta$ and the curve with $R = 5$ mm overlap.

$$\nabla^2\Psi_S + k_S^2\Psi_S = \frac{1}{4\pi V_S^2 r[(\rho_1\tilde{\rho}_{22} - \tilde{\rho}_{12}\rho_2)/\tilde{\rho}_{22}]}, \tag{17}$$

then the solution of Eq. (16) can be obtained by

$$u = -\nabla \times \nabla \times (K\Psi_S). \tag{18}$$

Solving Eq. (17), we may obtain

$$\Psi_S = C_S G_S(r) + \frac{1}{4\pi\omega^2 r[(\rho_1\tilde{\rho}_{22} - \tilde{\rho}_{12}\rho_2)/\tilde{\rho}_{22}]}. \tag{19}$$

The first term on the right-hand side of Eq. (19) is the general solution of the homogeneous equation $\nabla^2\Psi_S + k_S^2\Psi_S = -\delta_0$, and the second term on the right-hand side of Eq. (19) is the particular solution of the inhomogeneous equation. Note that

$$G_S(r) = \frac{e^{-ik_S r}}{4\pi r}. \tag{20}$$

The constant C_S is found from the regularity condition at the source point,

$$C_S = -\frac{1}{\omega^2[(\rho_1\tilde{\rho}_{22} - \tilde{\rho}_{12}\rho_2)/\tilde{\rho}_{22}]}. \tag{21}$$

Applying divergence operator to Eq. (14), and combining with Eq. (12), we obtain

$$\frac{1}{(\rho_1+\rho_2\xi_2)V_2^2}\nabla^2\nabla\cdot u_1 + \frac{1}{(\rho_1+\rho_2\xi_1)V_1^2}\nabla^2\nabla\cdot u_2 + \frac{k_1^2}{(\rho_1+\rho_2\xi_2)V_2^2}\nabla\cdot u_1 + \frac{k_2^2}{(\rho_1+\rho_2\xi_{12})V_1^2}\nabla\cdot u_2 = \frac{1}{4\pi(\rho_1+\rho_2\xi_2)V_2^2(\rho_1+\rho_2\xi_1)V_1^2}\nabla^2\nabla\cdot\left(\frac{K}{r}\right), \tag{22a}$$

$$\frac{1}{(\rho_{12}+\rho_{22}\xi_2)V_2^2}\nabla^2\nabla\cdot u_1 + \frac{1}{(\rho_{12}+\rho_{22}\xi_1)V_1^2}\nabla^2\nabla\cdot u_2 + \frac{k_1^2}{(\rho_{12}+\rho_{22}\xi_2)V_2^2}\nabla\cdot u_1 + \frac{k_2^2}{(\rho_{12}+\rho_{22}\xi_{12})V_1^2}\nabla\cdot u_2 = 0. \tag{22b}$$

Similarly, if there exist scalar potential functions Ψ_1 and Ψ_2 that satisfy

$$\nabla^2\Psi_i + k_i^2\Psi_i = \frac{1}{4\pi V_i^2 r(\rho_1+\rho_2\xi_i)}, \quad i = 1, 2, \tag{23}$$

then the sum of solutions u_1 and u_2 of Eq. (22) can be expressed by

$$u_1 + u_2 = \lambda_1\nabla\nabla\cdot(K\Psi_1) + \lambda_2\nabla\nabla\cdot(K\Psi_2), \tag{24}$$

where $k_i = \omega/V_i$ ($i = 1, 2$). From Eq. (22), we can see that λ_1 and λ_2 satisfy the following two equations

$$\begin{cases} \lambda_1 + \lambda_2 = 1 \\ \dfrac{\lambda_1}{(\tilde{\rho}_{12}+\tilde{\rho}_{22}\xi_2)(\rho_1+\rho_2\xi_1)} + \dfrac{\lambda_2}{(\tilde{\rho}_{12}+\tilde{\rho}_{22}\xi_1)(\rho_1+\rho_2\xi_2)} = 0. \end{cases} \tag{25}$$

We can easily find that

$$\begin{cases} \lambda_1 = \dfrac{(\tilde{\rho}_{12}+\tilde{\rho}_{22}\xi_2)(\rho_1+\rho_2\xi_1)}{(\tilde{\rho}_{12}+\tilde{\rho}_{22}\xi_2)(\rho_1+\rho_2\xi_1) - (\tilde{\rho}_{12}+\tilde{\rho}_{22}\xi_1)(\rho_1+\rho_2\xi_2)} \\ \lambda_2 = \dfrac{-(\tilde{\rho}_{12}+\tilde{\rho}_{22}\xi_1)(\rho_1+\rho_2\xi_2)}{(\tilde{\rho}_{12}+\tilde{\rho}_{22}\xi_2)(\rho_1+\rho_2\xi_1) - (\tilde{\rho}_{12}+\tilde{\rho}_{22}\xi_1)(\rho_1+\rho_2\xi_2)}. \end{cases} \tag{26}$$

The wave-fields described by Eq. (22) are divergent fields, so Ψ_1 and Ψ_2 are two potential functions of two dilatational waves, i.e., the fast- and slow-compressional waves. λ_1 and λ_2 in Eq. (24) are the contributions of Ψ_1 and Ψ_2 to the displacement field, respectively.

Figs. 7 and 8 show that the variations of λ_1 and λ_2 with different parameters. The effect of the parameter R on λ_1 and λ_2 is very weak. In the high-frequency range, the viscoelastic parameter $\tan\delta$ has different effects on

the coefficients λ_1 and λ_2. Moreover, because $V_1^2 \gg V_2^2$, these terms about u_1 are much larger than those terms about u_2 in Eq. (22), resulting in $|\lambda_1| \gg |\lambda_2|$ in the Green's function.

The solutions Ψ_1 and Ψ_2 of Eq. (23) can be written as a sum of particular plus general solutions,

$$\Psi_i = a_i G_i(r) + \frac{1}{4\pi\omega^2 r(\rho_1 + \rho_2\xi_i)}, \tag{27}$$

where

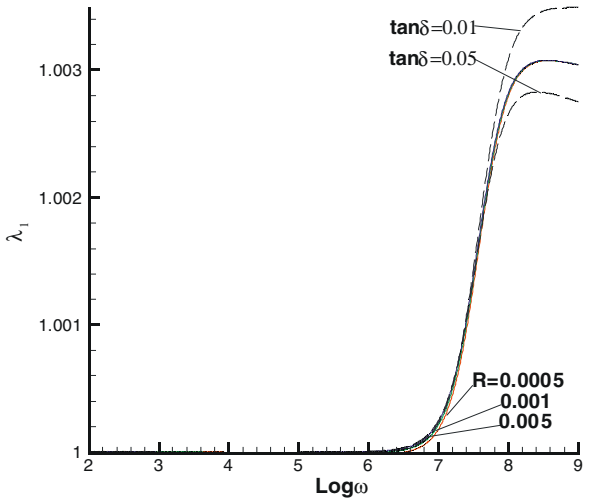

Fig. 7. Contribution of the potential function of fast P-waves to the Green's function. Different solid lines correspond to different values of R with $\tan\delta = 0.035$; different dashed lines correspond to different values of $\tan\delta$ with $R = 5$ mm. If R is not given in a figure, it means that the curves for the value of R and the curve with $\tan\delta = 0.035$ overlap. If $\tan\delta$ is not given in a figure, it means that the curves for different values of $\tan\delta$ and the curve with $R = 5$ mm overlap.

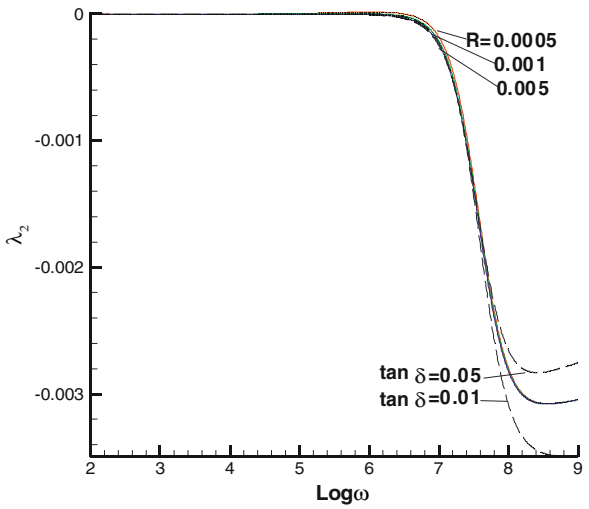

Fig. 8. Contribution of the potential function of slow P-waves to the Green's function. Different solid lines correspond to different values of R with $\tan\delta = 0.035$; different dashed lines correspond to different values of $\tan\delta$ with $R = 5$ mm. If R is not given in a figure, it means that the curves for the value of R and the curve with $\tan\delta = 0.035$ overlap. If $\tan\delta$ is not given in a figure, it means that the curves for different values of $\tan\delta$ and the curve with $R = 5$ mm overlap.

$$G_i(r) = \frac{e^{-ik_i r}}{4\pi r}, \quad a_i = -\frac{1}{\omega^2(\rho_1 + \rho_2 \xi_i)}. \quad i = 1, 2. \tag{28}$$

Combining Eqs. (18) and (24), we can obtain the solution for Eq. (14) as

$$u = \lambda_1 \nabla\nabla \cdot (a_1 K G_1(r)) + \lambda_2 \nabla\nabla \cdot (a_2 K G_2(r)) - \nabla \times \nabla \times (C_S K G_S(r)) = G(x, \varsigma; \omega) \cdot K, \tag{29}$$

where $G(x, \varsigma; \omega)$ is the Fourier transform of the Green's displacement function, and is given by

$$\begin{aligned} G(x, \varsigma; \omega) = & \frac{1}{4\pi\omega^2} \left\{ \frac{\lambda_1}{(\rho_1 + \rho_2 \xi_1)} \left[\nabla\nabla \cdot \left(I \frac{e^{-ik_1 r}}{r} \right) \right] + \frac{\lambda_2}{(\rho_1 + \rho_2 \xi_2)} \left[\nabla\nabla \cdot \left(I \frac{e^{-ik_2 r}}{r} \right) \right] \right. \\ & \left. - \frac{1}{(\rho_1 \tilde{\rho}_{22} - \tilde{\rho}_{12} \rho_2)/\tilde{\rho}_{22}} \left[\nabla \times \nabla \times \left(I \frac{e^{-ik_S r}}{r} \right) \right] \right\} \end{aligned} \tag{30}$$

where $\boldsymbol{I}$ is the second-rank unit tensor.

4. Discussions and conclusions

Based on the viscoelastic BISQ theory, which represents both the Biot-flow mechanism and the squirt-flow mechanism in two-phase porous isotropic viscoelastic media, we have investigated the effects of the squirt-flow mechanism and viscoelasticity on wave propagation, and derived the Green's function of displacement fields.

Our results show the phase velocity and attenuation of S-waves and fast P-waves strongly depend on the viscoelasticity of solid phases. At the same time, the phase velocity and attenuation of fast P-waves are also affected by the squirt-flow mechanism. For the attenuation Q_1^{-1} variation with frequency of fast P-waves, there exist two peaks. The fact that the amplitudes of fast P-waves are in the same phase and the amplitudes of slow P-waves are in the opposite phase is an important reason that there exist fast P-waves and slow P-waves. In the low-frequency range, the squirt-flow characteristic length, not the viscoelasticity, influences the phase velocity of slow P-waves; it is opposite in the high-frequency range.

From Eqs. (24) and (26), λ_1 and λ_2, which, respectively, correspond to the contributions of fast compressional wave potential function Ψ_1 and slow-compressional wave potential function Ψ_2 to the Green's function, relate not only to both the Biot-flow mechanism and the squirt-flow mechanism, but also to the viscoelasticity of the solid phase. The fact that $V_1^2 >> V_2^2$ results in $|\lambda_1| \gg |\lambda_2|$ in the Green's function.

Acknowledgement

We thank the Editor David Hills and two anonymous reviewers for their constructive comments and we also thank David Booth of British Geological Survey for his corrections that lead to the significant improvements of this paper. This work was supported by the National Natural Science Foundation of China (Grant No.: 40574014 and 40574058). The work of EL was supported by the British Geological Survey and this paper is published with the permission of the Executive Director of the British Geological Survey (NERC).

References

Biot, M.A., 1956. Theory of propagation of elastic waves in a fluid-saturated porous solid. I. Low-frequency range, II. Higher frequency range. J. Acoust. Soc. Am. 28, 168–191.

Cheng, Y.F., Yang, D.H., Yang, H.Z., 2002. Biot/Squirt model in viscoelastic porous media. Chinese Phys. Lett. 19, 445–448.

Ding, B.Y., Ding, C.H., Meng, F.L., 2001. The Green's function on two-phase saturated medium by concentrated force. Acta Mech. Sinica 33, 234–241.

Dravinski, M., Zheng, T., 2000. Numerical evaluation of three-dimensional time-harmonic Green's functions for a nonisotropic full-space. Wave Motion 32, 141–151.

Dvorkin, J., Nur, A., 1993. Dynamic poroelasticity: a unified model with the squirt and the Biot mechanisms. Geophysics 58, 524–533.

Kazi-Aoual, M.N., Bonnet, G., Jouanna, P., 1988. Green's functions in an infinite transversely isotropic saturated poroelastic medium. J. Acoust. Soc. Am. 84, 1883–1889.

Liu, E., Zhang, Z.J., 2001. Numerical study of elastic wave scattering by distributed cracks or cavities using the boundary integral method. J. Comput. Acoust. 9, 1039–1054.

Liu, E., Zhang, Z.J., Zhang, L.B., 2002. Anisotropic BEM formulation of multiple scattering of elastic waves by distributed inclusions. In: Proc. 3rd Int. Conf. on Boundary Element Techniques (BeTeQ), Sept., 2002, Beijing, China. Tsinghua University Press and Springer-Verlag, pp. 39–44.

Mavko, G., Nur, A., 1975. Melt squirt in the asthenosphere. J. Geophys. Res. 80, 1444–1448.

Norris, A.N., 1985. Radiation from a point source and scattering theory in a fluid saturated porous solid. J. Acoust. Soc. Am. 77, 2012–2023.

Spies, M., 1997. Green's tensor function for Lamb's problem: the general anisotropic case. J. Acoust. Soc. Am. 102, 2438–2441.

Tewary, V.K., 1998. Inversion of elastic waveform data in anisotropic solids using the delta-function representation of the Green's function. J. Acoust. Soc. Am. 104, 1716–1719.

Yang, D.H., Zhang, Z.J., 2000. Effects of the Biot and the squirt-flow coupling interaction on anisotropic elastic waves. Chinese Sci. Bull. 45, 2130–2138.

Yang, D.H., Zhang, Z.J., 2002. Poroelastic wave equation including the Biot/squirt mechanism and the solid/fluid coupling anisotropy. Wave Motion 35, 223–245.